JEM Journal of Experimental Medicine

ARTICLE

ARID5B regulates metabolic programming in human adaptive NK cells

Frank Cichocki[1]*, Cheng-Ying Wu[1]*, Bin Zhang[1], Martin Felices[1], Bianca Tesi[2,3], Katie Tuininga[1], Phillip Dougherty[1], Emily Taras[1], Peter Hinderlie[1], Bruce R. Blazar[4], Yenan T. Bryceson[5,6], and Jeffrey S. Miller[1]

Natural killer (NK) cells with adaptive immunological properties expand and persist in response to human cytomegalovirus. Here, we explored the metabolic processes unique to these cells. Adaptive CD3$^-$CD56^{dim}CD57$^+$NKG2C$^+$ NK cells exhibited metabolic hallmarks of lymphocyte memory, including increased oxidative mitochondrial respiration, mitochondrial membrane potential, and spare respiratory capacity. Mechanistically, we found that a short isoform of the chromatin-modifying transcriptional regulator, AT-rich interaction domain 5B (ARID5B), was selectively induced through DNA hypomethylation in adaptive NK cells. Knockdown and overexpression studies demonstrated that ARID5B played a direct role in promoting mitochondrial membrane potential, expression of genes encoding electron transport chain components, oxidative metabolism, survival, and IFN-γ production. Collectively, our data demonstrate that ARID5B is a key regulator of metabolism in human adaptive NK cells, which, if targeted, may be of therapeutic value.

Introduction

Natural killer (NK) cells comprise a lineage of lymphocytes that function at the interface between innate and adaptive immunity (Vivier et al., 2011). They are important mediators of immunosurveillance and can eradicate susceptible infected and neoplastic cells through the targeted release of cytotoxic granules (Kägi et al., 1994). Recent studies of murine CMV infection have demonstrated that distinct subsets of NK cells can expand and persist long-term. These NK cells display hallmark features of adaptive T and B cells, including heightened effector functions and robust recall responses relative to nonadaptive subsets (Sun et al., 2009). In both mice and humans, "adaptive" NK cell expansion is associated with improved antiviral and antitumor activity (Cichocki et al., 2016; Nabekura and Lanier, 2016; Redondo-Pachón et al., 2017).

In humans, we and others have reported on unique subsets of human CMV (HCMV)–associated NK cells with a genome-wide DNA methylation profile similar to that of effector CD8$^+$ T cells. These adaptive NK cells display DNA methylation–dependent silencing of the transcription factor promyelocytic leukemia zinc finger and stochastic silencing of genes encoding the membrane proximal signaling molecules FcεRγ, SYK, and/or EAT-2 (Lee et al., 2015; Schlums et al., 2015). Adaptive NK cell populations expressing the activating receptor NKG2C expand and persist in response to HCMV infection in healthy donors (Gumá et al., 2004) and HCMV reactivation in hematopoietic cell transplant (HCT) recipients (Foley et al., 2012). The majority of NKG2C$^+$ NK cells in the peripheral blood of HCMV-seropositive individuals coexpress the maturation marker CD57 (Lopez-Vergès et al., 2011). Thus, HCMV infection drives a remarkable degree of heterogeneity within the NK cell population. Whether adaptive NK cells can be considered true "memory" lymphocytes in the same regard as T and B cells, or whether they represent a type of "trained innate" immunity described for monocyte-to-macrophage differentiation (Saeed et al., 2014), is still a matter of debate.

Mounting evidence suggests that adaptive NK cell subsets have a survival and/or self-renewal advantage over canonical NK cells. Adaptive NK cells that expand in response to HCMV reactivation in HCT recipients are stable at high frequencies out to at least 2 yr after transplant (Foley et al., 2012; Cichocki et al., 2016), and epigenetically unique populations of adaptive NK cells in healthy HCMV-seropositive donors appear to persist at stable frequencies for at least 35 mo (Lee et al., 2015; Schlums et al., 2015). Further evidence for enhanced persistence/survival of adaptive NK cells comes from analysis of patients with par-

[1]Department of Medicine, University of Minnesota, Minneapolis, MN; [2]Childhood Cancer Research Unit, Department of Women's and Children's Health, Karolinska Institutet, Karolinska University Hospital Solna, Stockholm, Sweden; [3]Clinical Genetics Unit, Department of Molecular Medicine and Surgery, and Center for Molecular Medicine, Karolinska Institutet, Karolinska University Hospital Solna, Stockholm, Sweden; [4]Department of Pediatrics, University of Minnesota, Minneapolis, MN; [5]Centre for Hematology and Regenerative Medicine, Department of Medicine, Karolinska Institutet, Karolinska University Hospital Huddinge, Stockholm, Sweden; [6]Broegelmann Research Laboratory, Department of Clinical Sciences, University of Bergen, Bergen, Norway.

*F. Cichocki and C.-Y. Wu contributed equally to this paper; Correspondence to Jeffrey S. Miller: mille011@umn.edu.

oxysmal nocturnal hemoglobinuria, in which adaptive NK cells typically represent a lineage that predates the acquired hematopoietic stem cell *PIGA* mutations that progressively dominate hematopoiesis and production of canonical NK cells (Corat et al., 2017). Moreover, adaptive NK cells persist in the peripheral blood of patients with heterozygous *GATA2* mutations, where constitutive differentiation of progenitor and canonical NK cells is lost (Schlums et al., 2017).

The mechanistic basis for enhanced adaptive NK cell persistence is unclear. In particular, little is known regarding the metabolic attributes associated with adaptive NK cells that arise in response to HCMV infection. Bioenergetic profiling of T cells has revealed that memory $CD8^+$ T cell metabolism is characterized by increased utilization of oxidative phosphorylation (OXPHOS), an oxygen-dependent process that maximizes the amount of ATP that can be derived from substrates. Memory T cells also exhibit a characteristic increase in mitochondrial mass, which is associated with higher spare respiratory capacity (SRC) relative to naive or effector T cell populations (van der Windt et al., 2012, 2013).

Here, we show that adaptive NK cells from HCMV-seropositive individuals exhibit enhanced oxidative and glycolytic metabolic profiles relative to canonical NK cells. Adaptive NK cells also had increased mitochondrial membrane potential and higher expression of multiple genes encoding components of the mitochondrial ATP synthase complex and electron transport chain (ETC) relative to canonical NK cells. Mechanistically, we show that adaptive NK cells express elevated levels of the chromatin-modifying protein AT-rich interaction domain 5B (ARID5B). Knockdown of ARID5B in an NK cell line (NK-92) led to decreases in mitochondrial oxidative metabolism, expression of ETC genes, survival, and IFN-γ production. Conversely, overexpression of ARID5B in NK-92 cells led to increases in oxidative metabolism and IFN-γ production. Furthermore, we found that ARID5B directly regulates expression of the ETC component ubiquinone–cytochrome c reductase-binding protein (UQCRB), and UQCRB knockdown phenocopied the metabolic and functional effects observed for ARID5B knockdown. Thus, we demonstrate an important role for ARID5B in regulating NK cell metabolism.

Results

Adaptive NK cells from HCMV-seropositive donors exhibit elevated glycolytic and oxidative metabolism

To study how metabolism is regulated in NK cells that arise and persist in response to HCMV infection, we isolated NK cells from HCMV-seropositive and -seronegative donors and measured O_2 consumption rates (OCR) at the basal state, after the addition of oligomycin (an inhibitor of ATP synthesis), carbonyl cyanide-4 (trifluoromethoxy) phenylhydrazone (FCCP; uncouples ATP synthesis from the ETC), and rotenone and antimycin A, which interfere with complex I and complex III of the ETC, respectively (Gerencser et al., 2009). We found that maximal respiration levels, ATP-linked respiration, and SRC were significantly elevated in NK cells from HCMV-seropositive donors (Fig. 1 a). To determine whether observed increases in measures of OXPHOS were associated with the frequency of adaptive $CD3^-CD56^{dim}CD57^+NKG2C^+$ NK cells, we phenotyped NK cells from all HCMV-seropositive and -seronegative donors tested. As expected, adaptive NK cells were present in HCMV-seropositive donors at higher frequencies (7.5–32.1%) relative to seronegative donors (1.32–4.33%; P = 0.034). Strong correlations were observed between the magnitude of maximal respiration, ATP-linked respiration, and SRC and the frequencies of adaptive NK cells (Fig. 1 e).

A previously published, modified version of the Seahorse technology where glucose and pyruvate are added along with OXPHOS reagents in the same assay to maximize metabolic readouts from limited numbers of primary NK cells (Marçais et al., 2014) was used to measure the extracellular acidification rate (ECAR), which is an indication of glycolysis. No statistically significant differences were observed between NK cells from HCMV-seropositive and -seronegative donors with respect to maximal glycolysis and glycolytic reserve (Fig. 1 c). Weaker correlations were evident between the magnitude of maximal glycolysis and glycolytic reserve and the frequencies of adaptive NK cells (Fig. 1 e). We also observed higher ATP levels in NK cells from HCMV-seropositive donors with adaptive NK cell expansions relative to NK cells from HCMV-seronegative donors in direct ATP quantification assays (Fig. 1 b).

To investigate which nutrient source supports the increase in ATP levels observed in NK cells from HCMV-seropositive donors, we pretreated NK cells from HCMV-seronegative and -seropositive donors with etomoxir (to block fatty acid transport into the mitochondria), 2DG (to block glycolysis), and UK5099 (to block pyruvate transport into the mitochondria) before ATP quantification. As expected, both etomoxir and 2DG decreased ATP levels in NK cells relative to vehicle controls. However, no differences between HCMV-seronegative and -seropositive donors were observed. Interestingly, UK5099 pretreatment induced more substantial decreases in ATP production in NK cells from HCMV-seropositive donors compared with seronegative donors, suggesting that mitochondrial utilization of glucose plays a role in supporting the enhanced metabolism of adaptive NK cells (Fig. 1 d).

To directly analyze metabolic responses in distinct NK cell subsets, we sorted canonical NK cells and adaptive NK cells from HCMV-seropositive donors and performed Seahorse assays. In these experiments, we observed markedly enhanced OCR profiles for adaptive NK cells with significant elevations in maximal respiration, ATP-linked respiration, and SRC relative to canonical NK cells (Fig. 1 f). Similarly, adaptive NK cells showed higher ECAR profiles with elevated maximal glycolysis and glycolytic reserve relative to canonical NK cells (Fig. 1 g). Higher ATP levels were also observed in sorted adaptive NK cells relative to canonical NK cells (Fig. 1 h). To confirm the differences between isolated canonical and adaptive NK cells with respect to glycolytic metabolism, we performed glucose uptake assays using the fluorescent glucose analogue 2-NBDG. We observed significantly more glucose uptake in adaptive NK cells in response to triggering through CD16 as well as activation using PMA:ionomycin (Fig. 1 i). Of note, Seahorse experiments were either performed with freshly isolated NK cells or NK cells from peripheral blood mononuclear cells (PBMCs) that had previously been frozen. In direct comparisons, though maximal respiration was lower in

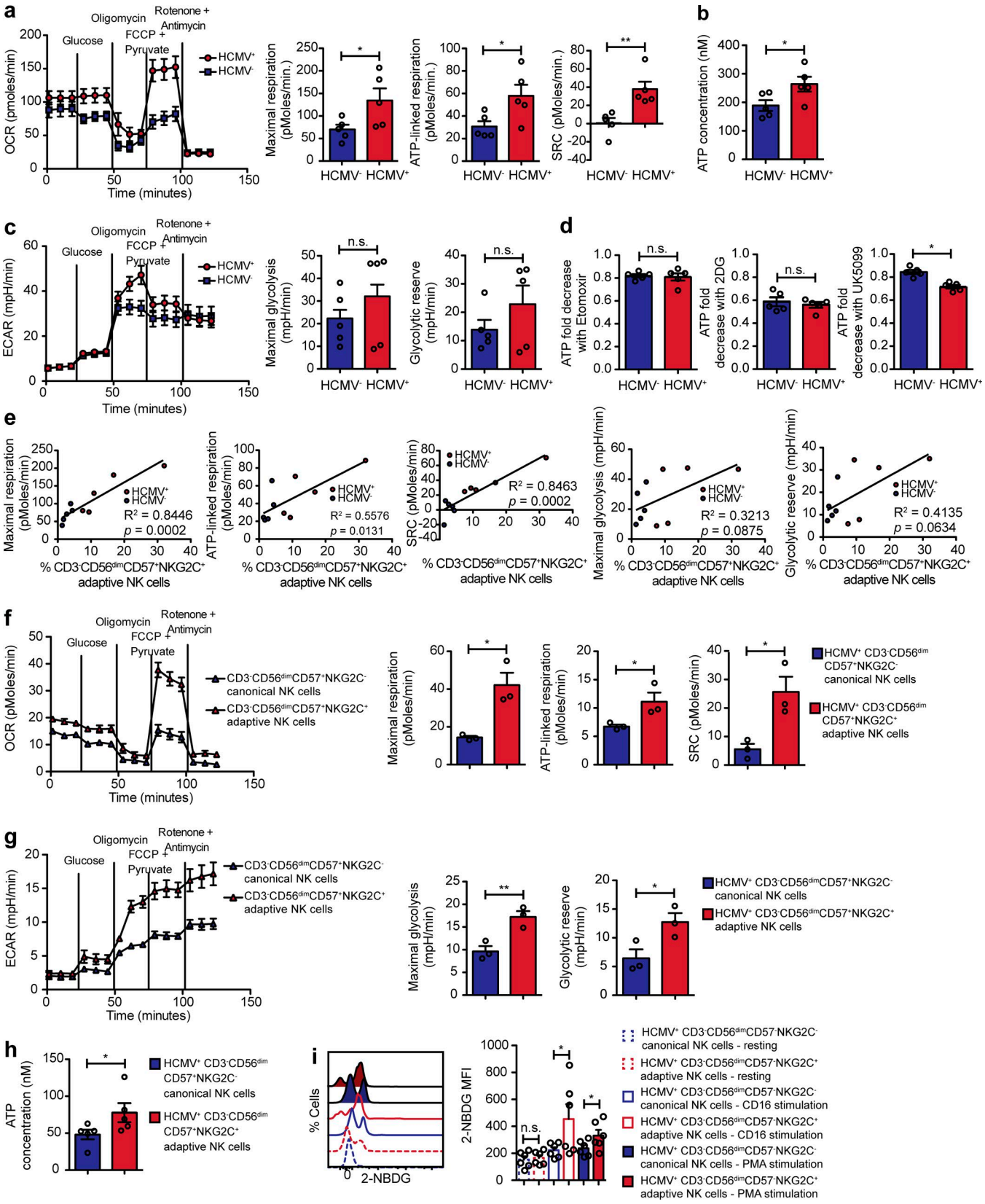

Figure 1. **Adaptive NK cells exhibit heightened glycolysis and mitochondrial oxidative metabolism. (a)** Metabolic functions in freshly isolated NK cells from five HCMV-seropositive and five HCMV-seronegative donors were analyzed by Seahorse. Shown are OCR profiles for representative donors and averages for maximal respiration, ATP-linked respiration, and SRC. **(b)** Quantification of ATP in NK cells from four seronegative and four seropositive donors. **(c)** ECAR profiles for representative donors and averages for maximal glycolysis and glycolytic reserve. **(d)** NK cells were isolated from five seronegative and five seropositive donors and incubated with the indicated inhibitors for 10 min before lysis and ATP quantification. Shown are fold decreases in ATP for each inhibitor

frozen cells, the overall OCR and ECAR profiles were similar (Fig. S1). Together, these data suggest that both mitochondrial oxidative metabolism and glycolysis are enhanced in adaptive NK cells from HCMV-seropositive donors.

Adaptive NK cells display increased mitochondrial membrane potential and expression of genes encoding components of the ETC

One of the most striking findings from our metabolic analyses was the dramatic increase in SRC in adaptive NK cells from HCMV-seropositive donors. SRC is a measure of how efficiently the ETC can shuttle protons from the mitochondrial matrix into the intermembrane space in response to the ATP synthesis uncoupling agent FCCP relative to the basal state (Mookerjee et al., 2010) and is considered to be a reflection of the ability of cells to produce energy in response to increased work or stress (Nicholls, 2009). Elevated SRC is associated with increased mitochondrial mass and a memory phenotype in $CD8^+$ T cells (van der Windt et al., 2012, 2013). To determine whether differences in mitochondrial membrane potential were evident between subsets of canonical and adaptive NK cells, we isolated NK cells from HCMV-seropositive and -seronegative donors and stained with fluorescently conjugated antibodies against CD57 and NKG2C for FACS analysis (Fig. 2 a) along with MitoTracker Deep Red, a fluorescent cell-permeable dye that relies on mitochondrial membrane potential ($\Delta\psi m$; Perry et al., 2011). We observed similar staining intensity in canonical NK cell subsets from HCMV-seronegative and -seropositive donors. In contrast, adaptive NK cell subsets exhibited increased mitochondrial membrane potential (Fig. 2 b). This increase was also evident when we sorted canonical and adaptive NK cells and analyzed mitochondria by confocal microscopy (Fig. 2 c). We confirmed increased mitochondrial levels in adaptive NK cells by quantification of the ratio of mitochondrial DNA to nuclear DNA by quantitative RT-PCR (qRT-PCR). We observed an 81% increase in the mitochondrial DNA ratio in adaptive NK cells (Fig. 2 d). Of note, no relative increase in the levels of ROS, as determined by CellRox staining, was observed in adaptive NK cells (Fig. 2 e).

To gain a deeper understanding with respect to the observed increases in OXPHOS and mitochondrial membrane potential in adaptive NK cells, we sorted canonical and adaptive NK cell subsets from the peripheral blood of five HCMV-seropositive donors and performed RNA-sequence (RNA-seq) analyses. Intriguingly, we observed a consistent pattern of increased expression of genes encoding components of the mitochondrial ATP synthase complex and ETC complexes I, III, and IV in adaptive NK cell subsets (Fig. 2 f). Among the most differentially expressed genes in this subset were *NDUFS4*, *NDUFS5*, and *NDUFB5* (encoding components of ETC complex I) and *UQCRH* and *UQCRB* (encoding components of ETC complex III). We validated the differential expression of these genes by sorting peripheral blood canonical and adaptive NK cells from HCMV-seropositive donors and performing qRT-PCR. We observed a statistically significant increase in the expression of each of these genes in adaptive NK cells relative to canonical NK cells (Fig. 2 g). Gene set enrichment analysis (GSEA) of the RNA-seq data also showed a statistically significant enrichment of genes involved in lipid catabolism in adaptive NK cells, consistent with previous reports (Liu et al., 2017), and a trend toward enrichment of genes involved in mitochondrial biogenesis and fatty acid metabolism (Table S1). Together, these data establish a unique metabolic profile characteristic of adaptive NK cells.

Expression of the chromatin-modifying protein ARID5B is induced in adaptive NK cells

Several transcription factors and chromatin-modifying proteins have been implicated in mitochondrial biogenesis and cellular oxidative metabolism, including members of the nuclear receptor superfamily, the peroxisome proliferator-activated receptors (Puigserver et al., 1998), and the estrogen-related receptors (Huss et al., 2004). In our RNA-seq analysis of gene expression from freshly isolated NK cells, we observed similar expression levels of peroxisome proliferator-activated receptor and estrogen-related receptor family members when comparing canonical and adaptive NK cell subsets. We also observed similar expression levels of other genes encoding known transcriptional regulators of mitochondrial biogenesis and OXPHOS, including *YY1*, *MYC*, *TFAM*, *TFB2M*, and *TFB1M* (Larsson et al., 1998; Falkenberg et al., 2002; Li et al., 2005; Cunningham et al., 2007; Fig. S2). However, our analysis revealed higher expression of *ARID5B* specifically in adaptive versus canonical NK cells (1.7-fold, adjusted P = 0.013; Fig. 3 a). ARID5B belongs to a family of proteins that share a unique DNA-binding domain designated AT-rich interactive domain (ARID; Kortschak et al., 2000). Knockout mice are viable at reduced frequencies, exhibit markedly stunted growth, and are abnormally lean (Lahoud et al., 2001; Whitson et al., 2003). Although the immune system has not been studied in depth in these mice, abnormalities in B cell and T cell development, including significant decreases in bone marrow and thymic cellularities, have been reported (Falkenberg et al., 2002). Because ARID5B has been implicated in the direct regulation of metabolism in hepatocytes (Baba et al., 2011), direct regulation of inflammatory and lipid metabolism pathways in human $CD14^+$ blood monocytes (Liu et al., 2017), and indirectly in the regulation of adipose cell

relative to vehicle controls. **(a–d)** Results are from two independent experiments. **(e)** Associations between Seahorse metabolic readouts and the percentages of adaptive NK cells. Unpaired Student's *t* tests were used to determine statistical significance. **(f)** Adaptive and canonical NK cells from three seropositive donors were sorted and analyzed by Seahorse. Shown is the OCR profile from a representative donor and averages for maximal respiration, ATP-linked respiration, and SRC. **(g)** Shown is the ECAR profile of canonical and adaptive NK cells from a representative donor, as well as the averages for maximal glycolysis and glycolytic reserve. All OCR and ECAR results are from two independent experiments. **(h)** Quantification of ATP in sorted canonical NK cells and adaptive NK cells from five seropositive donors. **(i)** Measurement of glucose uptake using 2-NBDG in isolated NK cells from six seropositive donors at rest, after stimulation with an anti-CD16 antibody and after stimulation with PMA:ionomycin. Shown are the 2-NBDG mean fluorescence intensity (MFI) averages in gated canonical and adaptive NK cells in each condition. Results are from two independent experiments. Paired Student's *t* tests were used to determine statistical significance. Error bars represent SEM. *P < 0.05, **P < 0.01. n.s., not significant.

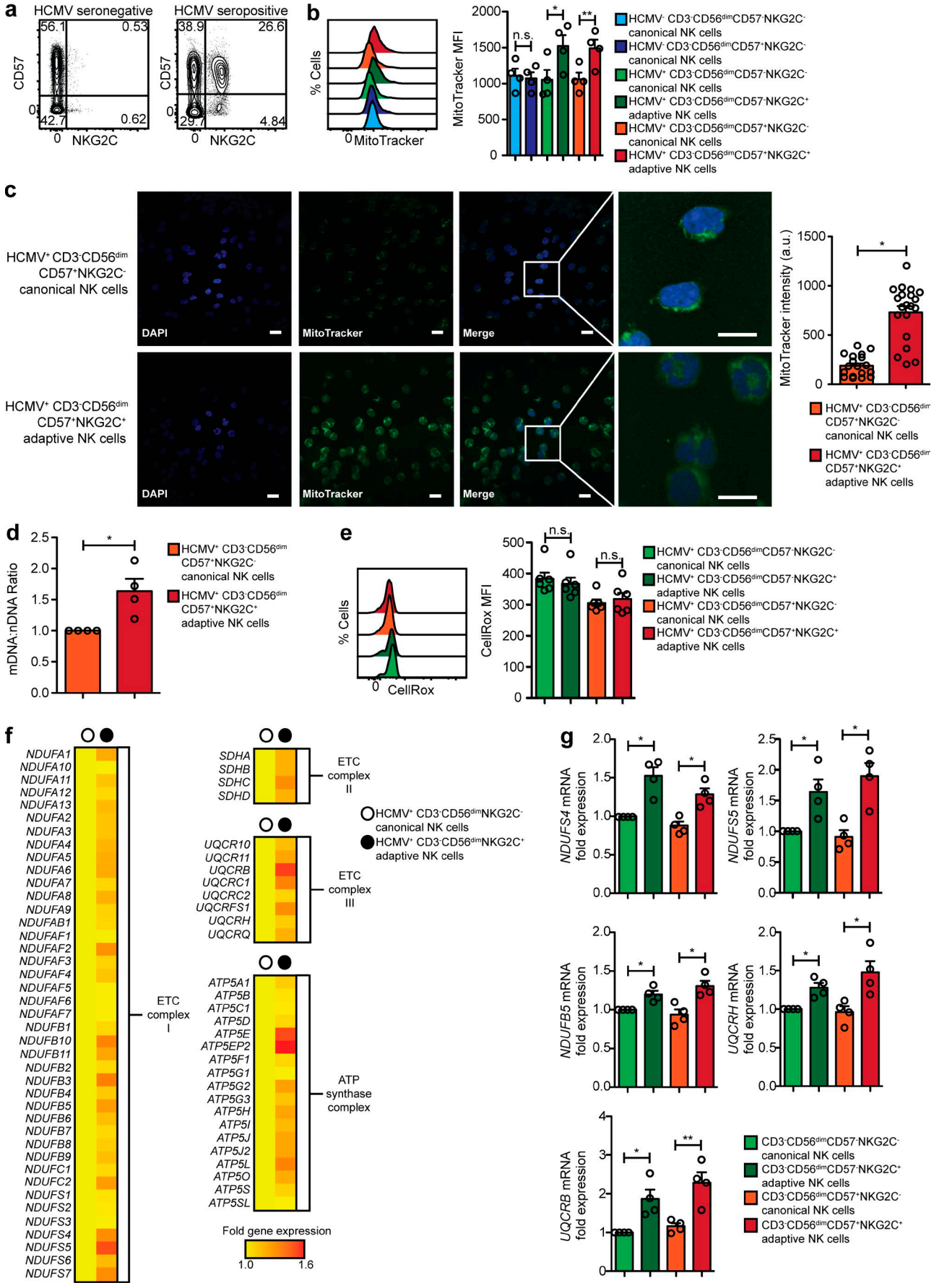

metabolism through control of the *FTO* locus (Claussnitzer et al., 2015), we hypothesized that ARID5B also plays a role in regulating NK cell metabolism.

Increased expression of *ARID5B* in adaptive NK cells was confirmed by qRT-PCR using sorted subsets of canonical and adaptive NK cells from HCMV-seropositive donors (Fig. 3 b). Two *ARID5B* isoforms have previously been identified: transcript variant 1 consists of 10 exons spanning 149,402 bp on chromosome 10, and transcript variant 2 has a unique first exon located within intron 4 of transcript variant 1 and shares the final six exons. To quantitatively visualize splice junctions and the relative expression of each isoform in canonical and adaptive NK cells, we used the Mixture of Isoforms package within the Integrative Genomics Viewer software to create Sashimi plots of our RNA-seq alignment data. We found that *ARID5B* transcript variant 2 was enriched in adaptive NK cells (Fig. 3 c). To confirm ARID5B variant expression at the protein level, we sorted canonical NK cells and adaptive NK cells from HCMV-seropositive donors and performed Western blots for ARID5B. Interestingly, ARID5B variant 2 was more abundant than variant 1 in both canonical and adaptive NK cells. The expression of both variants was higher in adaptive NK cells, with variant 2 being most abundant (Fig. 3 d).

To determine whether there was a unique epigenetic signature in adaptive NK cells associated with the pattern of *ARID5B* expression, we examined data from our genome-wide DNA methylation arrays previously performed with sorted subsets of canonical and adaptive NK cells (Schlums et al., 2015). While the 5′ region and transcriptional start site (TSS) upstream of *ARID5B* transcript variant 1 were hypomethylated to a similar extent in canonical and adaptive NK cells, we observed selective hypomethylation of the 5′ region and TSS upstream of *ARID5B* transcript variant 2 in adaptive NK cells ($P = 2.32 \times 10^{-12}$; Fig. 3 e). Together, our data show a specific induction of ARID5B in adaptive NK cells with an enrichment of variant 2.

ARID5B modulation impacts mitochondrial membrane potential, mitochondrial oxidative metabolism, IFN-γ production, and survival in NK-92 cells

To test the hypothesis that ARID5B promotes NK cell metabolism, we knocked down ARID5B expression in the NK-92 NK cell line via lentiviral transduction. By this method, we were able to achieve a 40% reduction in ARID5B expression (Fig. 4 a). Mitochondrial membrane potential, as quantified by MitoTracker, was reduced by 38% in ARID5B knockdown NK-92 cells (Fig. 4 b), and similar results were observed when cells were visualized by confocal microscopy (Fig. 4 c). Decreased mitochondrial membrane potential was observed in NK-92 cells transduced with three different shRNAs targeting ARID5B (Fig. S3). To further confirm that ARID5B knockdown affected mitochondrial levels, we quantified the ratio of mitochondrial DNA to nuclear DNA by qRT-PCR and found that this ratio was reduced by 31% in ARID5B knockdown cells (Fig. 4 d).

Next, we sought to determine whether knockdown of ARID5B had an effect on metabolism. Significant reductions in maximal respiration, ATP-linked respiration, and SRC were observed for ARID5B knockdown cells (Fig. 4 e). In contrast, no overall differences were seen in glycolysis as determined by the ECAR profile of ARID5B knockdown cells, and both maximal glycolysis and glycolytic reserve were similar between ARID5B knockdown cells and controls (Fig. 4 f). ATP levels were also similar between ARID5B knockdown cells and controls (Fig. 4 g). Elevated mitochondrial mass, OXPHOS, and SRC are associated with superior T cell effector function (van der Windt et al., 2012, 2013; Buck et al., 2016). To determine whether ARID5B knockdown impacted NK cell function, we stimulated control and ARID5B knockdown NK-92 cells overnight with the inflammatory cytokines IL-12 and IL-18 to induce IFN-γ production. We observed a marked impairment of IFN-γ production by ARID5B knockdown NK-92 cells (Fig. 4 h). Of note, no differences in degranulation or TNF production were observed between control and ARID5B knockdown cells in K562 stimulation assays (not shown).

A role for ARID5B in supporting survival of T-ALL cell lines has been recently reported (Leong et al., 2017). We hypothesized that ARID5B may play a similar role in NK cells. To test this hypothesis, we performed cell cycle analyses using propidium iodide and found an accumulation of ARID5B knockdown cells in G1 relative to controls with a trend toward a decreased frequency of cells in G2 (Fig. 5 a). Analysis of viable cell counts over 3 d in culture showed a significantly decreased growth rate for ARID5B knockdown cells (Fig. 5 b). To determine whether the impaired growth of ARID5B knockdown cells could be due to decreased survival, we analyzed active apoptosis using annexin V. We observed a higher frequency of ARID5B knockdown cells undergoing apoptosis (Fig. 5 c). As the inner mitochondrial membrane protein BCL-2 plays a key role in blocking programmed cell death (Sentman et al., 1991), and adaptive NK cells express elevated lev-

Figure 2. **Adaptive NK cells have increased mitochondrial membrane potential and expression of ETC genes. (a)** Representative FACS plots of CD57 and NKG2C on gated NK cells from seronegative and seropositive donors. **(b)** Representative histogram plots of MitoTracker staining within the indicated NK cell subsets (left) and cumulative data of MitoTracker MFI values from five seronegative donors and five seropositive donors (right). **(c)** Canonical and adaptive NK cells were sorted from two seropositive donors in two independent experiments, stained with MitoTracker and DAPI dyes, and analyzed by confocal microscopy. Shown are representative images from one donor (left) and cumulative MitoTracker intensity values from 18 canonical NK cells and 20 adaptive NK cells (right). Scale bars are 10 µm. a.u., arbitrary units. **(d)** qRT-PCR was used to determine the ratio of mitochondrial DNA to genomic DNA for canonical and adaptive NK cells. Results are from four donors in two independent experiments. **(e)** Representative FACS histogram plots of CellRox staining in the indicated subsets of NK cells from a HCMV-seropositive donor (left) and cumulative data of CellRox MFI values from six donors in two independent experiments (right). **(f)** The indicated subsets of canonical and adaptive NK cells were sorted from five seropositive donors in three independent experiments and used for RNA-seq analysis. Shown is a heat map of normalized fold-expression values for mitochondrial ATP synthase complex and ETC genes in canonical and adaptive NK cells. **(g)** The indicated subsets of canonical and adaptive NK cells were sorted from four seropositive donors in two independent experiments and used for qRT-PCR. All expression values were normalized against *ACTB* and against gene expression values from $CD3^-CD56^{dim}CD57^-NKG2C^-$ canonical NK cells. Error bars represent SEM. Paired Student's *t* tests were used to determine statistical significance. *P < 0.05, **P < 0.01. n.s., not significant.

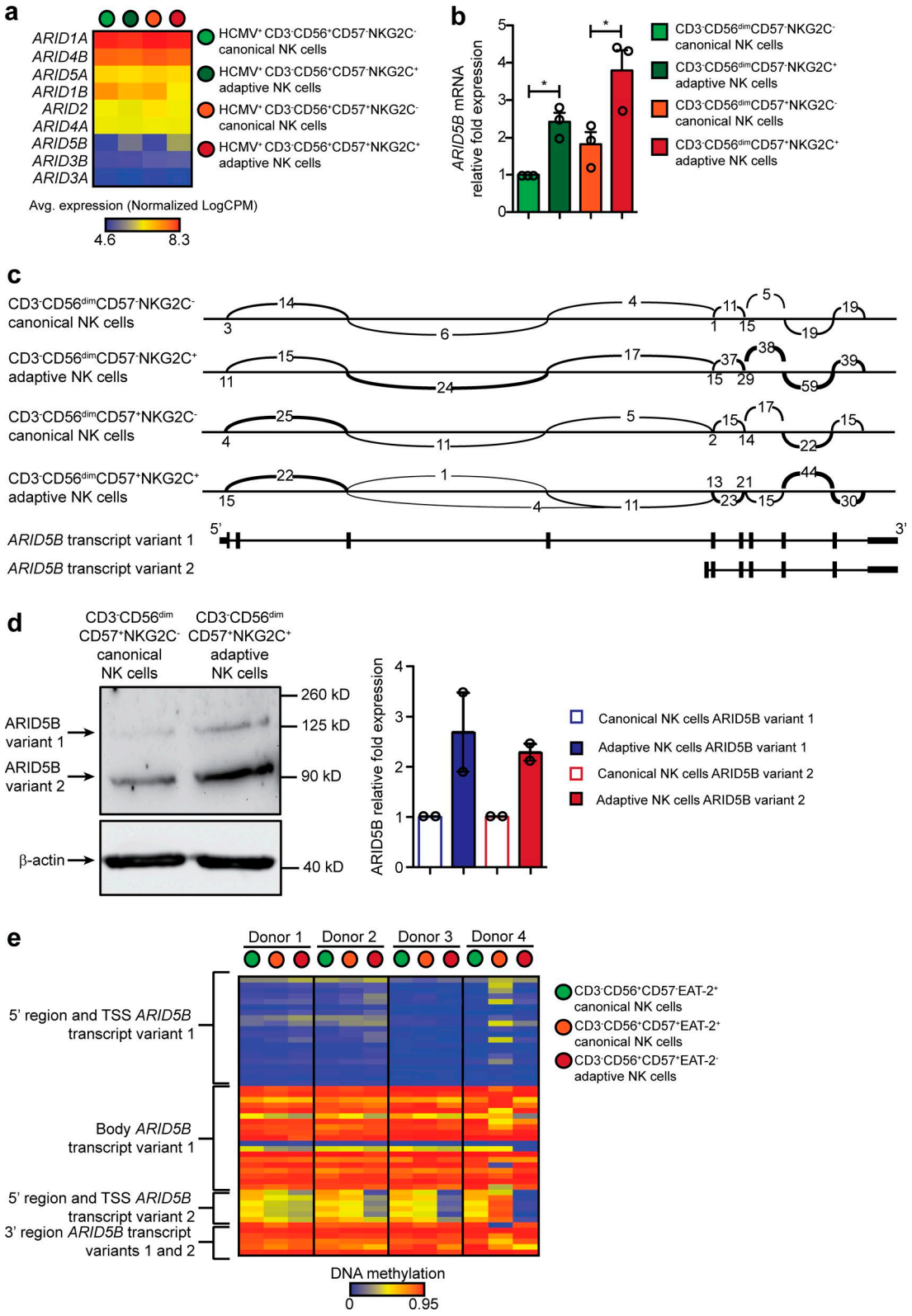

Figure 3. **ARID5B expression is elevated in adaptive NK cells. (a)** Shown is a heat map of average normalized expression of genes belonging to the ARID family from the RNA-seq dataset. **(b)** Cumulative qRT-PCR data of *ARID5B* mRNA expression in the indicated canonical and adaptive NK cell subsets sorted from three HCMV-seropositive donors. All expression values were normalized against *ACTB*, and fold-expression values were determined for each subset relative to $CD3^-CD56^{dim}CD57^-NKG2C^-$ canonical NK cells. Results are from two independent experiments. **(c)** Sashimi plots of RNA-seq data from a representative donor showing genomic alignments of RNA-seq reads and splice junctions within the *ARID5B* locus. **(d)** Canonical and adaptive NK cells were sorted from two seropositive donors in two independent experiments. Western blots were performed with antibodies against ARID5B and β-actin. Shown is a representative

els of BCL-2 (Zhang et al., 2013), we analyzed BCL-2 expression in control and ARID5B knockdown cells by Western blot. Interestingly, we observed a 44% reduction in BCL-2 expression in ARID5B knockdown cells (Fig. 5 d).

In addition to shRNA-mediated knockdown experiments, we also overexpressed ARID5B variant 2 in NK-92 cells via lentiviral transduction using the pCDH vector containing a GFP cassette and the open reading frame for ARID5B variant 2. We observed a 1.62-fold increase in ARID5B in cells transduced with the overexpression vector relative to the empty vector control (Fig. 6 a). ARID5B overexpression in NK-92 cells resulted in a 1.31-fold increase in mitochondrial membrane potential (Fig. 6 b). Additionally, we transduced primary NK cells with the control and ARID5B overexpression vectors. We observed a 1.57-fold increase in mitochondrial membrane potential in cells overexpressing ARID5B (Fig. 6 c). NK-92 cells overexpressing ARID5B exhibited higher maximal respiration and SRC, as determined by Seahorse analysis (Fig. 6 d), but no statistically significant differences in glycolytic metabolism (Fig. 6 e) or ATP levels (Fig. 6 f) were observed. Functionally, ARID5B-overexpressing cells had higher frequencies of IFN-γ production in response to overnight IL-12 and IL-18 stimulation (Fig. 6 g). Together, these data suggest that ARID5B influences mitochondrial membrane potential, oxidative mitochondrial metabolism, survival, and IFN-γ production.

ARID5B directly regulates expression of the ETC complex III component UQCRB, and UQCRB knockdown phenocopies the metabolic and functional effects of ARID5B knockdown

Analysis of our RNA-seq data revealed a pattern of higher expression of several genes encoding components of the ETC in adaptive NK cell subsets (Fig. 2). We hypothesized that ARID5B could be directly or indirectly involved in the regulation of ETC genes. To test this hypothesis, we chose to study *UQCRB* in greater detail, since it had the highest statistical significance for differential expression between canonical and adaptive NK cells among all ETC genes in our RNA-seq analysis (1.46-fold, adjusted P = 0.037). UQCRB is a nucleus-encoded component of complex III in the mitochondrial respiratory chain, which plays an essential role in electron transfer for ATP production (Haut et al., 2003). To confirm elevated UQCRB expression in adaptive NK cells, we sorted canonical and adaptive NK cells from HCMV-seropositive donors and performed Western blots for UQCRB. In cells from both donors analyzed, UQCRB protein was strongly induced (1.97-fold) in adaptive NK cells (Fig. 7 a). We also confirmed reduced expression of UQCRB in ARID5B knockdown NK-92 cells at the mRNA (Fig. 7 b) and protein (Fig. 7 c) levels.

Next, we searched the promoter region immediately upstream of the *UQCRB* TSS for potential ARID5B binding sites. ARID5B has been shown to preferentially bind an AATA(C/T) core consensus sequence (Whitson et al., 1999). Three such motifs were identified in the promoter of *UQCRB* (Fig. 7 d). We then performed chromatin immunoprecipitation (ChIP) assays to analyze both polymerase II and ARID5B binding to the *UQCRB* promoter. A separate DNA sequence 1,728 bp upstream of the *UQCRB* TSS was included as a control for binding specificity in the assay. We found that both polymerase II and ARID5B bound to the *UQCRB* promoter in NK-92 cells, and binding was substantially diminished with ARID5B knockdown (Fig. 7 e). To determine whether ARID5B was enriched within the *UQCRB* promoter in primary adaptive NK cells, we sorted canonical and adaptive NK cells and performed ChIP assays to analyze ARID5B binding to the control site upstream of *UQCRB* and to the *UQCRB* promoter. We observed ARID5B binding to the *UQCRB* promoter but not the upstream site in both canonical and adaptive NK cells and a significant enrichment of ARID5B binding in adaptive NK cells (Fig. 7 f). ARID5B promotes gene expression through its interaction with plant homeodomain finger 2 (PHF2). The ARID5B–PHF2 complex is a specific histone demethylase complex that demethylates the inhibitory H3K9Me2 histone modification (Baba et al., 2011). To determine whether H3K9Me2 levels within the promoter of *UQCRB* were inversely correlated with ARID5B binding and UQCRB expression, we sorted primary canonical and adaptive NK cells and performed ChIP assays with an antibody specific for H3K9Me2. We observed significantly lower H3K9Me2 enrichment at the *UQCRB* promoter in adaptive NK cells (Fig. 7 g).

Given the direct regulation of UQCRB expression by ARID5B, we next sought to determine the metabolic and functional effects of UQCRB knockdown. To this end, we knocked down UQCRB expression in NK-92 NK cells via lentiviral transduction. By this method, we were able to achieve a 37% reduction in UQCRB expression (Fig. 8 a). Mitochondrial membrane potential was reduced by 33% in UQCRB knockdown NK-92 cells when analyzed by FACS (Fig. 8 b). Significant reductions in maximal respiration and SRC were observed for UQCRB knockdown cells (Fig. 8 c). In contrast, there was a trend toward increased glycolysis observed in UQCRB knockdown cells, though differences in maximal glycolysis and glycolytic reserve between UQCRB knockdown cells and controls were not statistically significant (Fig. 8 d). ATP levels were similar between UQCRB knockdown cells and controls (Fig. 8 e). Functionally, we observed a marked impairment of IFN-γ production by UQCRB knockdown NK-92 cells in response to IL-12 and IL-18 stimulation (Fig. 8 f). Overall, these data show that ARID5B directly controls UQCRB expression, and knockdown of UQCRB phenocopies ARID5B knockdown.

Discussion

We propose a model in which increased metabolism supports adaptive NK cell expansion and survival. The enhanced metabolism observed in adaptive NK cells appears to be dependent, at least in part, on increased expression of ARID5B and its induction of genes encoding components of the ETC, including the ETC complex III gene *UQCRB*. ARID5B also appears to play a signifi-

blot from one donor (left) and quantification by densitometry for both donors (right). **(e)** Methylation patterns throughout the *ARID5B* locus generated from whole-genome methylation profiling of the indicated canonical and adaptive NK cell populations sorted from four seropositive donors. Error bars represent SEM. Paired Student's *t* tests were used to determine statistical significance. *P < 0.05.

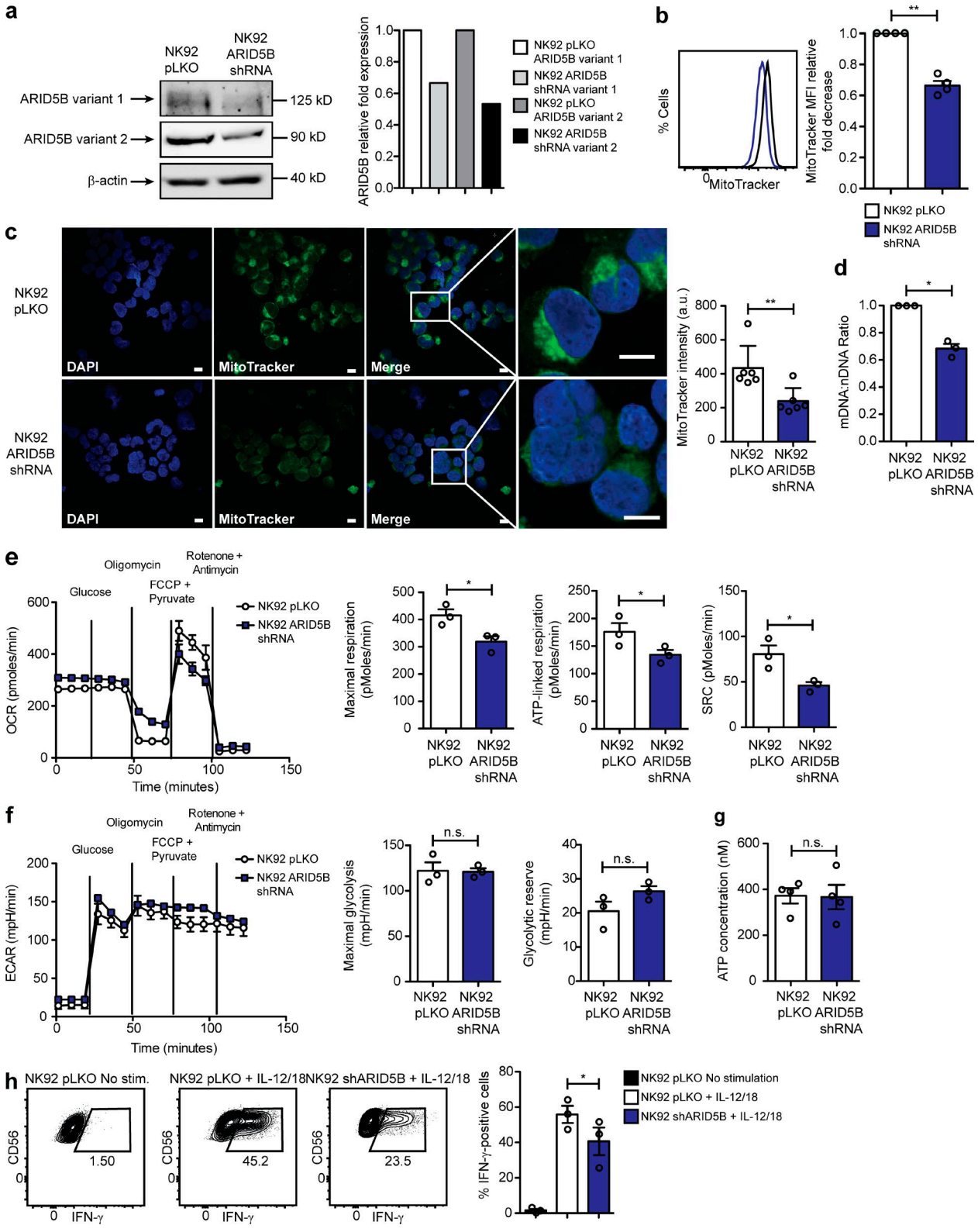

Figure 4. **Knockdown of ARID5B leads to a decrease in mitochondrial membrane potential, oxidative mitochondrial metabolism, and IFN-γ production.** NK-92 cells were transduced with an empty control pLKO.1 vector or a pLKO.1 vector containing an ARID5B-specific shRNA. **(a)** Western blot of ARID5B and β-actin in the control and shARID5B NK-92 lines (left) and quantification by densitometry (right). **(b)** Representative FACS plots (left) and cumulative fold differences in MitoTracker MFI values (right) from each indicated NK-92 cell line. Experiments were replicated twice. **(c)** The indicated NK-92 cell lines were stained with DAPI and MitoTracker dyes and visualized by confocal microscopy. Shown are representative images (left) and cumulative MitoTracker intensity values calculated from 11 individual cells (right). Scale bars are 10 µm. Results are from two independent replicates, with similar results observed in both experiments. a.u., arbitrary units. **(d)** qRT-PCR was used to determine the ratio of mitochondrial DNA to genomic DNA for each indicated NK-92 cell line. Results are from three independent replicates. **(e)** OCR profiles of the control and shARID5B NK-92 cell lines in a representative experiment and averages for maximal

cant role in NK cell survival, as ARID5B knockdown is associated with increased apoptosis and reduced BCL-2 expression. Because BCL-2 localization to the mitochondria counteracts the production of ROS, a byproduct of ETC activity (Giménez-Cassina and Danial, 2015), elevated BCL-2 in adaptive NK cells may be important to limit oxidative stress. Whether ARID5B directly regulates BCL-2 and other survival genes requires further investigation.

One caveat to the knockdown and overexpression studies presented here is that they were performed using NK-92 cells due to the difficulty of transducing or transfecting primary NK cells at high enough frequencies to use in metabolic and functional analyses. NK-92 cells, like all transformed cells, have significant metabolic alterations that could be confounding. That being said, our model is consistent with previous work showing that $CD8^+$ T cells lacking MCJ/DnaJC15, a repressor of respiratory chain activity, exhibit increased OXPHOS, more mitochondrial mass, enhanced survival during cytokine withdrawal, an increased ability to secrete IFN-γ, and superior control of viral infection (Champagne et al., 2016). The metabolic and functional effects of ARID5B on cytotoxic lymphocyte metabolism appear to be very similar to those reported for MJC/DnaJC15 loss. Our results are also consistent with recent work showing that ETC activity, but not ATP production, is essential for IFN-γ production in effector memory $CD8^+$ T cells (Bantug et al., 2018). We conclude that ARID5B can enhance aspects of NK cell metabolism and IFN-γ production by control of ETC gene expression.

Given our results showing increased expression of ARID5B in adaptive NK cells and a role for ARID5B in promoting OXPHOS and survival, it is possible that ARID5B plays a similar role in controlling metabolism and survival in T and B cell memory subsets. In support of this idea, transcript expression data from the Immunological Genome Project show an increase in ARID5B expression throughout human B cell maturation, with a marked increase in ARID5B expression in mature class-switched B cells relative to non–class-switched B cells. Similarly, both $CD4^+$ and $CD8^+$ central and effector memory T cells express significantly higher ARID5B transcript levels relative to naive subsets. As such, induction of ARID5B may represent a general mechanism supporting cellular persistence and immunological memory formation.

How ARID5B expression is induced in adaptive NK cells is unclear. We performed experiments in which NK cells were cultured with inflammatory cytokines (IL-15, IL-21, and IL-12) and CD16 or NKG2C agonist antibodies, but did not observe an induction of ARID5B. In fact, *ARID5B* transcript expression levels decreased during activation in vitro (Fig. S4). In transformed T cells, *ARID5B* is a downstream target of the oncogenic transcription factor T cell acute lymphocytic leukemia 1 (TAL1) and is required for the survival and growth of acute lymphoblastic leukemia T cells (Leong et al., 2017). Whether TAL1 can induce ARID5B expression in primary lymphocytes has yet to be determined.

Together, our results support the notion that adaptive NK cells that arise in response to HCMV infection have defined characteristics of immunological memory. Hallmarks of T cell memory, including increases in OXPHOS, SRC, and mitochondrial mass, are also evident in adaptive NK cells from HCMV-seropositive individuals. We identify ARID5B as a transcription factor that may promote the long-term persistence of adaptive NK cells after HCMV reactivation in HCT recipients and their enhanced ability to produce IFN-γ. Moreover, our results suggest that ARID5B may represent a common factor important to support recall responses to secondary infections. Strategies to increase ARID5B and therefore enhance mitochondrial function and NK cell persistence may be of therapeutic value in NK cell immunotherapy.

Materials and methods

Cell source

Typed HCMV-seropositive and HCMV-seronegative blood products drawn from healthy, consenting donors were purchased from Memorial Blood Bank (Minneapolis, MN). All samples were de-identified before receipt, and the institutional review board at the University of Minnesota approved these studies. All research was conducted in accordance with the Declaration of Helsinki. All blood samples were drawn with donor consent.

Primary cell isolation, cell lines, and culture

PBMCs were isolated by density gradient centrifugation using Ficoll-Paque Premium (GE Healthcare). For sorting experiments, T cells and B cells were depleted using anti-CD3 and anti-CD19 magnetic beads (STEMCELL Technologies). For phenotypic analyses, NK cells were isolated by negative selection using the EasySep Human NK Cell Isolation Kit (STEMCELL Technologies). Primary cells were cultured overnight in RPMI media (Gibco) supplemented with 10% FBS in the absence of cytokines. NK-92 and K562 cells were obtained from ATCC and cultured according to their instructions. The following cytokines were used in culture experiments: IL-15 (National Cancer Institute), IL-21 (eBiosciences), and IL-12 (R&D Systems). Plate-bound anti-NKG2C agonist antibody (a gift from J.P. Houchins at R&D Systems) was used in some culture experiments.

Flow cytometry and cell sorting

For flow cytometry, fluorochrome-conjugated antibodies to the surface epitopes CD3 (OKT4; Biolegend), CD56 (HDCD56; Biolegend), CD57 (NK-1; BD Biosciences), NKG2C (134591; R&D Systems), and CD107a (H4A3; BD Biosciences) were used. Intracellular EAT-2 was stained using a rabbit polyclonal antibody (Proteintech Group) followed by secondary staining with fluorochrome-conjugated anti-rabbit reagents (Invitrogen). Intracellular staining of cytokines was performed using fluo-

respiration, ATP-linked respiration, and SRC. **(f)** ECAR profiles for the indicated NK-92 cell lines in a representative experiment and averages for maximal glycolysis and glycolytic reserve. All cumulative OCR and ECAR results were replicated twice. **(g)** Quantification of ATP in control and shARID5B cell lines. **(h)** Control and shARID5B NK-92 cells were cultured overnight with and without IL-12 and IL-18 before FACS analysis of NK cell functional readouts. Representative FACS plots and cumulative data of the frequencies of IFN-γ expression by NK-92 cells are shown. **(g and h)** Experiments were replicated twice. Error bars represent SEM. Paired Student's *t* tests were used to determine statistical significance. *P < 0.05, **P < 0.01. n.s., not significant.

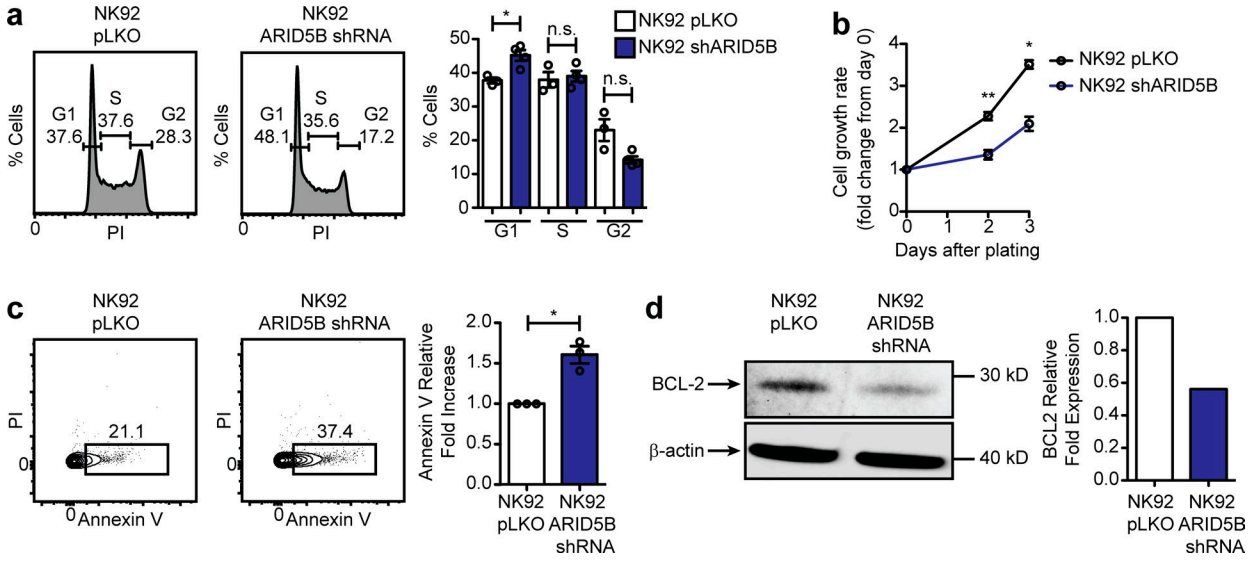

Figure 5. **Knockdown of ARID5B leads to reduced survival and expression of the pro-survival protein BCL-2. (a)** Cell cycle analysis of control and shARID5B NK-92 cells by propidium iodide staining (PI). Shown are representative FACS plots for both NK-92 lines (left) and cumulative data of the percentages of cells in each cell cycle phase (right). Experiments were replicated twice. **(b)** Control and shARID5B NK-92 cells were plated at equal numbers, and viable cell counts were taken after 2 and 3 d in culture. Shown is cumulative fold expansion data for both lines. Results are from four replicates in two independent experiments. **(c)** Control and shARID5B NK-92 cells were stained with annexin V and propidium iodide and analyzed by flow cytometry. Shown are representative FACS plots gated on lymphocytes (left) and cumulative fold differences (right). **(d)** Western blot of BCL-2 in control and shARID5B NK-92 cells. Shown is a representative blot (left) and fold decrease in shARID5B NK-92 cells calculated by densitometry (right). **(c and d)** Experiments were replicated twice. Error bars represent SEM. Paired Student's *t* tests were used to determine statistical significance. *P < 0.05, **P < 0.01. n.s., not significant.

rochrome-conjugated antibodies against IFN-γ (B27; BD Biosciences) and TNF (MAb11; Biolegend). For phenotypic analyses, PBMCs or purified NK cells were surface stained with the indicated antibodies along with a fixable dead cell stain (Invitrogen) in FACS buffer (PBS supplemented with 2% FBS and 2 mM EDTA) and fixed in 2% formaldehyde. For intracellular staining, cells were permeabilized in 0.05% Triton X-100 (Sigma). Flow cytometry data were acquired on an LSR II instrument (BD Biosciences) and analyzed with FlowJo (v10, Tree Star). MitoTracker Deep Red, CellRox (ThermoFisher), and propidium iodide (Sigma) staining was performed according the manufacturer's instructions. For sorting experiments, PBMCs were stained with the indicated antibodies and sorted to >95% purity on a FACS Aria II instrument (BD Biosciences).

Seahorse metabolism, ATP quantification, glucose uptake, and annexin V assays

Seahorse assays were performed according to the manufacturer's instructions with modifications to simultaneously analyze glycolysis and oxidative mitochondrial metabolism using the Seahorse XF Glycolysis Stress Test Kit and the Seahorse XF Cell Mito Stress Test Kit (Agilent Technologies). Briefly, NK cells were washed and resuspended in glucose-free media (Gibco). 10^6 cells per well were spun down onto plates coated with poly-L-lysine. Triplicate wells were set up for experiments using $CD3^-CD56^+$ NK cells isolated from bulk PBMCs and transduced NK-92 cells. Glucose, oligomycin, FCCP, sodium pyruvate, rotenone, and antimycin A were serially injected to measure metabolic function. Plates were analyzed using an XF^e 24 Extracellular Flux Analyzer (Agilent Technologies). For experiments using sorted primary NK cells, 5×10^5 cells from each population were plated in triplicate wells and analyzed using the same protocol above using an XF^e 96 Extracellular Flux Analyzer (Agilent Technologies). SRC measurements were calculated as average maximal OCR values minus average basal OCR values. ATP levels were calculated as average basal OCR values minus average postoligomycin OCR values. Glycolysis was calculated as average postglucose ECAR values minus average basal ECAR values. Glycolytic reserve was calculated as average maximal ECAR values minus postglucose ECAR values. For glucose uptake assays, NK cells were cultured with 10 ng/ml IL-15 alone ± anti-CD16 antibody (1 µg; 3G8; BD Biosciences) for 1 h or ± PMA (25 ng/ml) and ionomycin (1 µM; Sigma) for 15 min in media containing the fluorescently labeled glucose analogue 2-(*N*-(7-nitrobenz-2-oxa-1,3-diazol-4-yl)amino)-2-deoxyglucose (2-NBDG; Life Technologies) at a final concentration of 50 µM. For ATP quantification assays, 10^2 NK cells per well were assayed using the ATP Bioluminescence Assay Kit HS II (Sigma) and analyzed on an Infinite M200 PRO Luminometer (Tecan). For ATP assays using metabolic inhibitors, etomoxir (40 µM), 2DG (50 mM), and UK5099 (50 nM) (Sigma) were added 10 min before cell lysis and ATP determination. For cell apoptosis analysis, cells were stained with annexin V FITC and propidium iodide (ThermoFisher) according to the manufacturer's instructions.

Confocal microscopy

For mitochondria imaging experiments, cells were stained with MitoTracker Deep Red dye (ThermoFisher) according to the manufacturer's instructions. After staining, cells were washed three times with PBS and spun onto slides with a Cytospin 2 (Shandon). Cells were fixed and mounted in Vectashield with DAPI staining dye (Vector Labs). Images were acquired with an Olympus BX up-

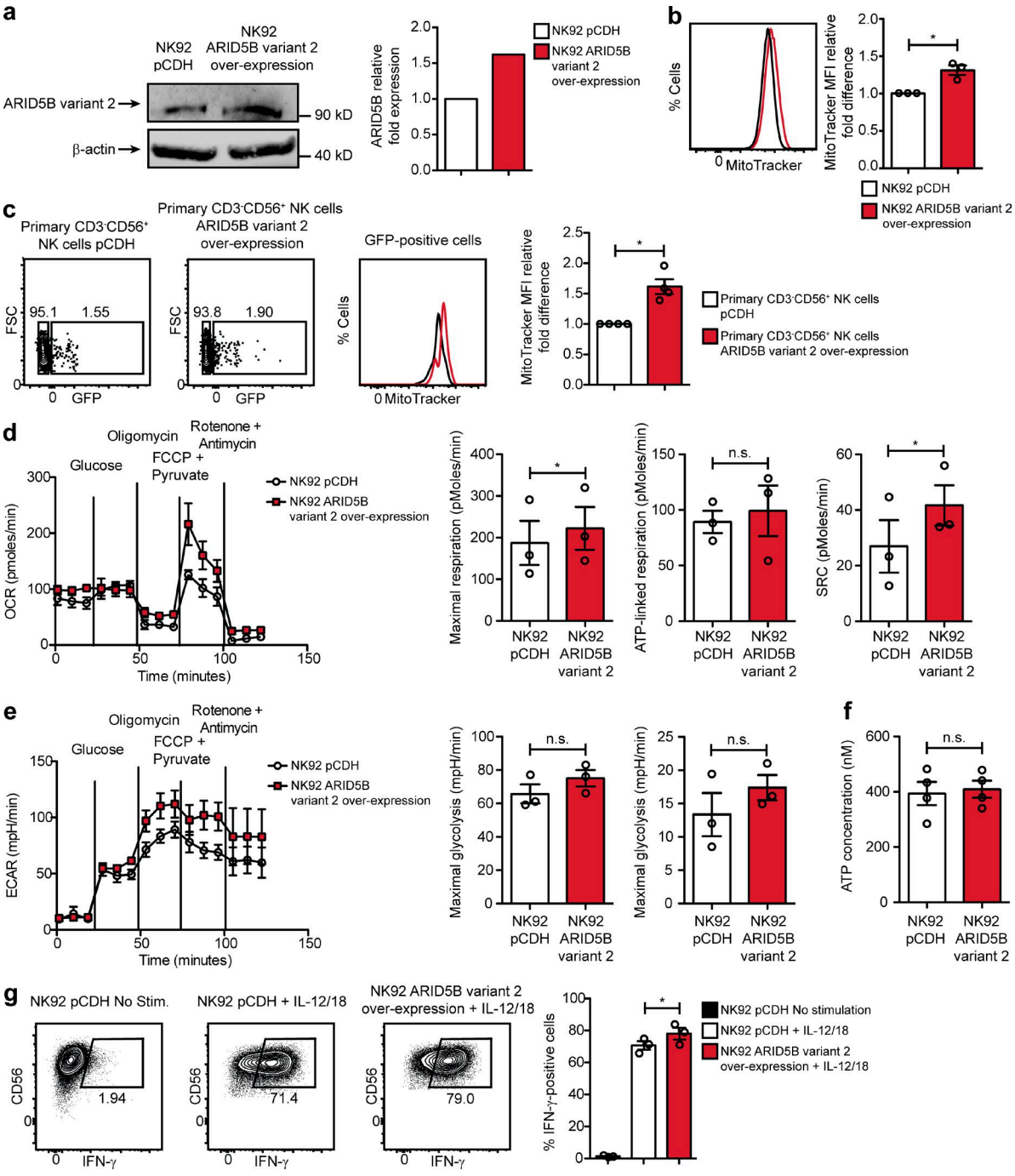

Figure 6. **Overexpression of ARID5B results in increases in mitochondrial membrane potential, oxidative mitochondrial metabolism, and IFN-γ production.** NK-92 cells were transduced with a control pCDH vector containing GFP or a pCDH vector containing GFP and ARID5B variant 2. **(a)** Western blot of ARID5B variant 2 and β-actin in each sorted GFP⁺ NK-92 cell line (left) and image quantification by densitometry (right). **(b)** Mitochondrial membrane potentials were determined by MitoTracker staining and FACS analysis in sorted GFP⁺ cells from the control and ARID5B variant 2 overexpression NK-92 lines. Cumulative data of the relative fold difference in MitoTracker staining between vectors are shown (right). Experiments were replicated twice. **(c)** Primary NK cells were transduced with the control or the ARID5B variant 2 overexpression vectors. Cells were analyzed for GFP expression and mitochondrial mass 72 h after transduction. Shown are representative FACS plots of GFP against forward scatter (FSC) in gated NK cells and MitoTracker histogram plots (left). Cumulative data from four donors of the relative fold difference in MitoTracker staining between vectors are also shown (right). Results are from two independent experiments. Similar results were observed in both experiments. **(d)** OCR profiles of the control and ARID5B variant 2–overexpressing NK-92 cell lines in a representative experiment and averages for maximal respiration, ATP-linked respiration, and SRC. **(e)** ECAR profiles for the indicated NK-92 cell lines in a representative experiment and averages for maximal glycolysis and glycolytic reserve. OCR and ECAR experiments were replicated twice. **(f)** Quantification of ATP in control and ARID5B-overexpressing cell lines in three independent replicates. **(g)** Control and ARID5B-overexpressing NK-92 cells were cultured overnight with and without IL-12 and IL-18 before FACS analysis. Representative FACS plots and cumulative data of the frequencies of IFN-γ expression by NK-92 cells are shown. Experiments were replicated twice. Error bars represent SEM. Paired Student's *t* tests were used to determine statistical significance. *P < 0.05. n.s., not significant.

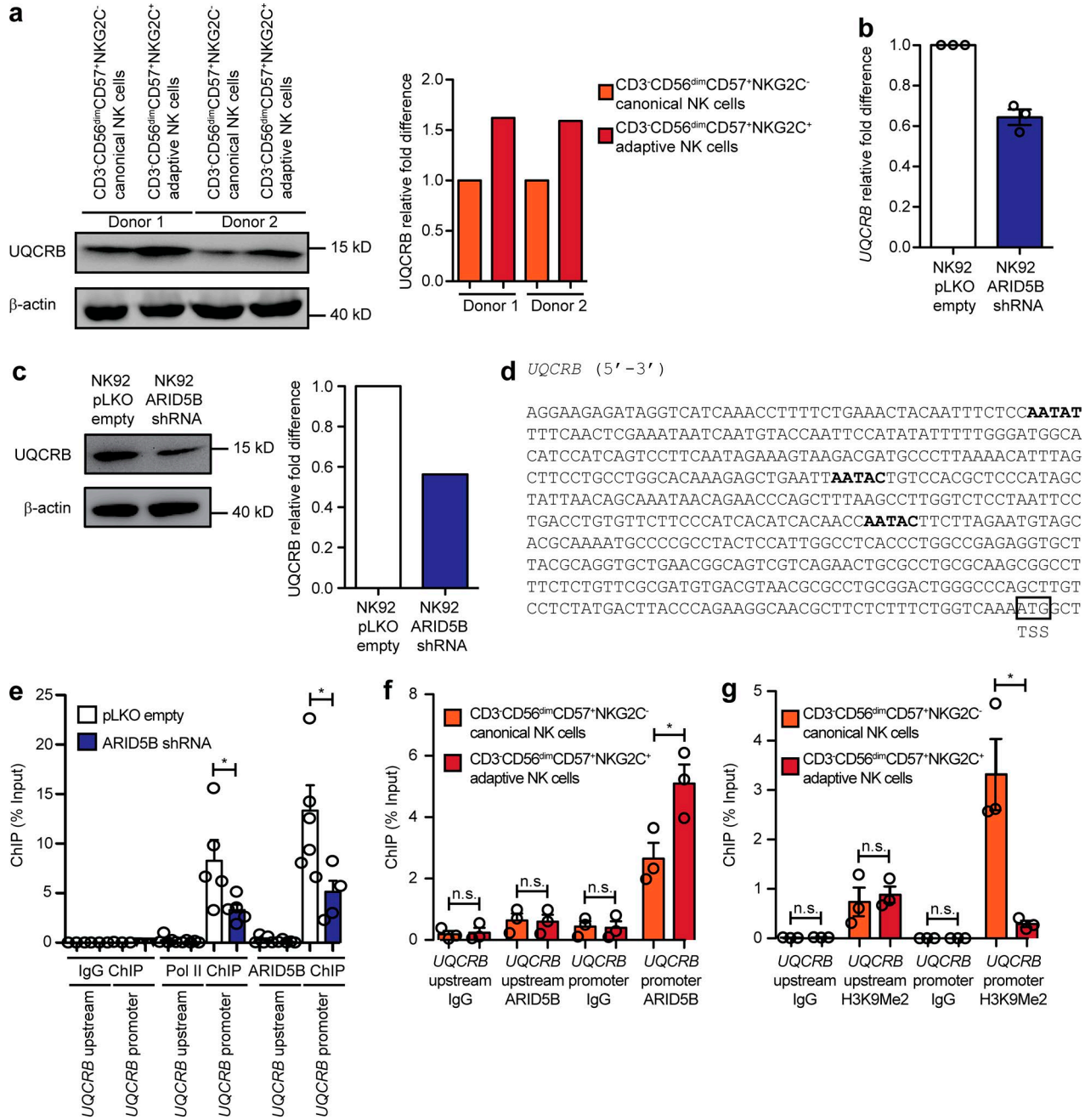

Figure 7. **ARID5B directly regulates UQCRB expression. (a)** Canonical and adaptive NK cells were sorted from two HCMV-seropositive donors and used for Western blot analysis of UQCRB (left). Quantification by densitometry and determination of fold difference is shown (right). **(b)** Determination of relative *UQCRB* mRNA in control versus shARID5B NK-92 cells by qRT-PCR. Results are from three independent experiments. **(c)** Western blot of UQCRB in the control and ARID5B knockdown NK-92 lines (left) and relative UQCRB expression calculated by densitometry (right). **(d)** Shown is the sequence of the upstream proximal promoter region of *UQCRB*. Putative core binding sites for ARID5B are highlighted in bold. The transcriptional start site (TSS) for *UQCRB* is also indicated. **(e)** Control and shARID5B NK-92 cells were used in ChIP assays to assess polymerase II and ARID5B binding to a control region far upstream of *UQCRB* (-1,728 bp) and to the proximal *UQCRB* promoter (-351 bp). The ChIP assays were repeated five times in three independent experiments. Results are shown as the percentage of input. **(f)** Canonical and adaptive NK cells were sorted from three HCMV-seropositive donors. Sorted cells were used in ChIP assays to assess ARID5B binding to the control region far upstream of *UQCRB* (-1,728 bp) and to the proximal *UQCRB* promoter (-351 bp). Results are from two independent experiments. **(g)** Canonical and adaptive NK cells were sorted from three HCMV-seropositive donors. ChIP assays were performed to assess H3K9Me2 levels in the control region far upstream of *UQCRB* and within the proximal *UQCRB* promoter. Control isotype IgG antibody was included in all assays as a control for nonspecific binding. Results are from two independent experiments. Error bars represent SEM. Paired Student's *t* tests were used to determine statistical significance. *P < 0.05. n.s., not significant.

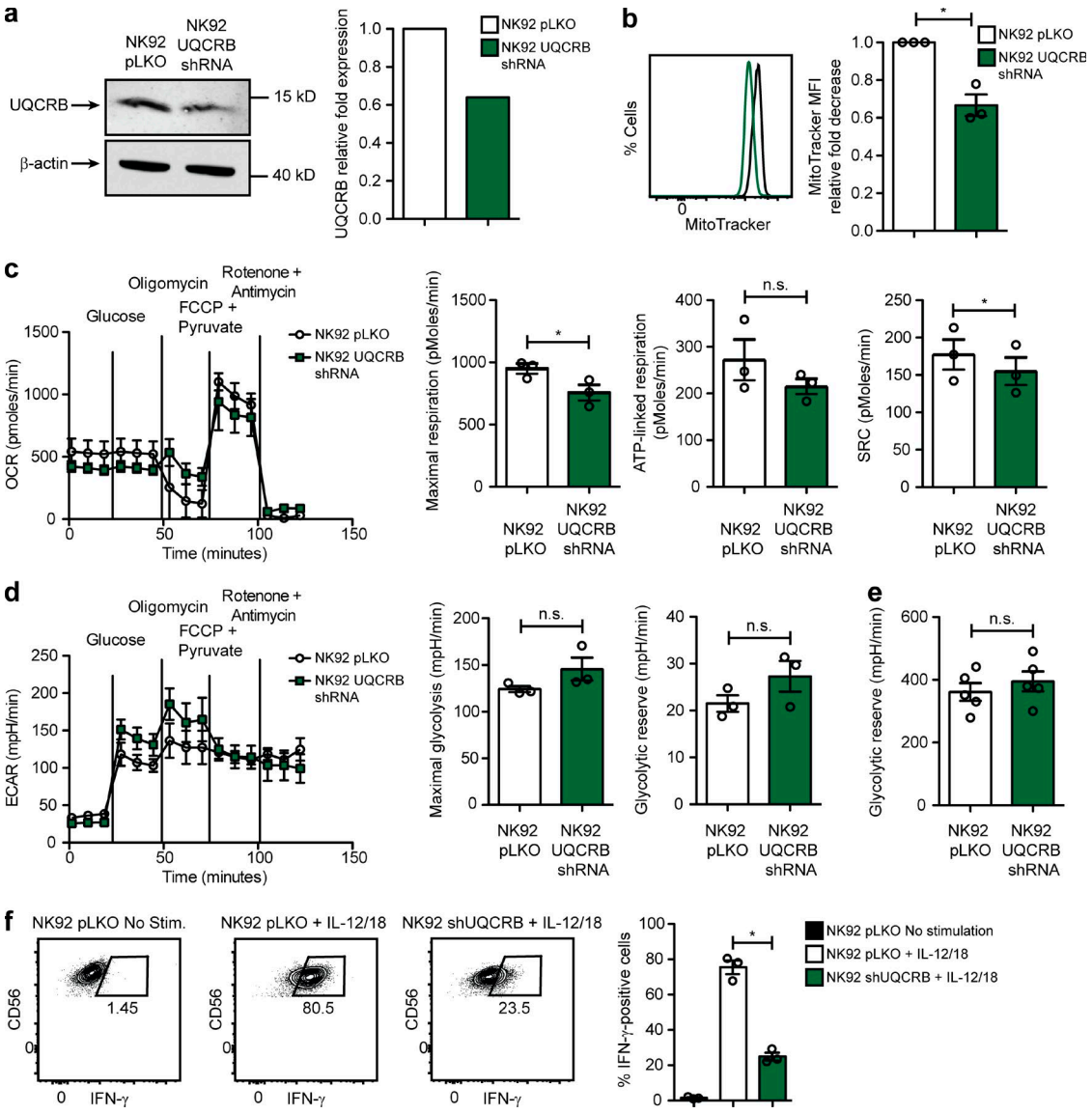

Figure 8. **Knockdown of UQCRB leads to a decrease in mitochondrial membrane potential, oxidative mitochondrial metabolism, and IFN-γ production.** NK-92 cells were transduced with an empty vector or a pLKO.1 vector containing UQCRB-specific shRNA. **(a)** Western blot of UQCRB and β-actin in the control and shUQCRB NK-92 lines (left) and quantification by densitometry (right). **(b)** Representative FACS plots (left) and cumulative fold differences in MitoTracker MFI values (right) from each indicated NK-92 cell line. Experiments were replicated twice. **(c)** OCR profiles of the control and shARID5B NK-92 cell lines in a representative experiment and averages for maximal respiration, ATP-linked respiration, and SRC. **(d)** ECAR profiles for the indicated NK-92 cell lines in a representative experiment and averages for maximal glycolysis and glycolytic reserve. All cumulative OCR and ECAR results were replicated twice. **(e)** Quantification of ATP in control and shUQCRB cell lines. **(f)** Control and shUQCRB NK-92 cells were cultured overnight with and without IL-12 and IL-18 before FACS analysis of NK cell functional readouts. Shown are representative FACS plots and cumulative data of the frequencies of IFN-γ expression by NK-92 cells. **(e and f)** Experiments were replicated twice. Error bars represent SEM. Paired Student's *t* tests were used to determine statistical significance. *P < 0.05. n.s., not significant.

right microscope equipped with a Fluoview 1000 confocal scan head with a 60× oil immersion objective (Olympus). Image processing and fluorescence intensity quantification was performed using Icy open platform software.

RNA-seq experiments

NK cells from the peripheral blood of HCMV-seropositive donors were analyzed by FACS for surface expression of CD3, CD56, CD57, and NKG2C and intracellular expression of FcεRγ, EAT-2, and SYK. Five donors were selected based on high adaptive CD56^{dim}CD57^{+}NKG2C^{+} NK cell frequencies (≥15% of all CD3^{-}CD56^{dim} NK cells) and lack of FcεRγ, EAT-2, and/or SYK specifically within the NKG2C^{+} population. Canonical CD3^{-}CD56^{dim}CD57^{-}NKG2C^{-} NK cells, canonical CD3^{-}CD56^{dim}CD57^{+}NKG2C^{-} NK cells, adaptive CD3^{-}CD56^{dim}CD57^{-}NKG2C^{+} NK cells, and adaptive CD3^{-}CD56^{dim}CD57^{+}NKG2C^{+} NK cells were sorted. RNA was extracted using an RNeasy Plus Micro Kit (Qiagen). Barcoded TruSeq RNA v2 libraries (Illumina) were created, and libraries were sequenced on a HiSeq 2500 (Illumina) as paired-end 100 bp. STAR version 2.4.0d was used to align the RNA-seq reads to the human genome reference

build GRCh37 (hg19). The Ensembl gene annotation version 75 was provided as gene transfer format for exon junction support. For each sample, reads were assigned to genes and summarized using featureCounts (subread package version 1.4.5-p1). Raw read counts were read into R (version 3.2.0) and subjected to normalization by the trimmed mean of M-values normalization method implemented in the R/bioconductor edgeR package and variance normalized using voom from the R/bioconductor limma package. All genes with at least one count per million (CPM) mapped reads in at least two samples were analyzed further. Differential gene expression was performed using the R/bioconductor limma package. RNA-seq data can be found under the GEO accession no. GSE117614.

Genome-wide DNA methylation analyses

The indicated NK cell subsets were sorted from the peripheral blood of HCMV-seropositive donors, and DNA was extracted using the DNeasy Blood & Tissue Kit (Qiagen). The EpiTect Bisulfite Kit (Qiagen) was used to convert unmethylated cytosines to uracils. Bisulfite-converted DNA was analyzed with the Infinium Human Methylation450 BeadChip platform (Illumina). A comprehensive description of the analysis pipeline with linked raw data has been published previously (Schlums et al., 2015).

Plasmids and retroviral transduction

All ARID5B shRNA, UQCRB shRNA, and control vectors (pLKO.1) were purchased from Open Biosystems. The shRNA targeting sequences from the three ARID5B clones tested were clone 1040, 5′-CCGGGCCTTCAAAGAGAACCATTTACTCGAGTAAATGGTTCTCTTTGAAGGCTTTTTTG-3′; clone 1281, 5′-CCGGCGATAGAACGAATACCCTATTCTCGAGAATAGGGTATTCGTTCTATCGTTTTTTG-3′; and clone 2853, 5′-CCGGCGAGGAAGAAACGAACGTGATCTCGAGATCACGTTCGTTTCTTCCTCGTTTTTTG-3′. The shRNA targeting sequence from the UQCRB clone tested was 5′-CCGGCCTAAAGAGCAGTGGACCAAACTCGAGTTTGGTCCACTGCTCTTTAGGTTTTTG-3′. ARID5B variant 2 overexpression vectors were created by cloning a custom gBlock gene fragment of the ARID5B variant 2 open reading frame (Integrated DNA Technologies) into the pCDH vector (Open Biosystems) by restriction digest using EcoR1 and BamH1 (New England Biolabs) and were transfected along with lentiviral packaging vectors into 293T cells using 1 µg/µl polyethylenimine (Polysciences). The sequence for ARID5B variant 2 (GenBank accession no. NM_032199) was from the GRCh37/hg19 genome assembly on the UCSC genome browser site (http://genome.ucsc.edu). Supernatants containing viral particles were used to transduce NK-92 cells or primary NK cells via spin transduction. Stable NK-92 lines were selected with puromycin (Sigma). For transduction experiments using primary NK cells, transduced cells were cultured for 48 h in a low concentration (1 ng/ml) of IL-15 before FACS analysis.

Western blot

Cells were lysed in ice-cold lysis buffer and run on 10% SDS-PAGE gels. Proteins were then transferred to nitrocellulose membranes and incubated at room temperature in 5% BSA in TTBS (50 mM Tris-HCl, 150 mM NaCl, and 0.05% Tween 20, pH 7.4) buffer for 1 h. Membranes were then incubated overnight with primary antibodies against ACTB (sc-47778; Santa Cruz Biotechnology), ARID5B (NBP1-83622; Novus Biologicals), BCL-2 (ab692; Abcam), or UQCRB (ab190360; Abcam) at a dilution of 1:1,000 in TTBS. Membranes were washed and incubated with anti-rabbit or anti-mouse horseradish peroxidase secondary antibodies at a 1:2,000 dilution for 1 h. Immunoreactive bands were imaged on a UVP Imaging System with enhanced chemiluminescence reagents (ThermoFisher). Densitometry analyses were performed using ImageJ software (National Institutes of Health).

qRT-PCR

For quantification of gene expression, cells were lysed in RLT buffer (Qiagen), and RNA was extracted using an RNeasy Plus Micro Kit (Qiagen). cDNA was synthesized from RNA using Superscript IV Reverse transcription (ThermoFisher). qRT-PCR reactions were performed using SYBR Green PCR Master Mix (Applied Biosystems). qRT-PCR–based assays for determining the ratio of mitochondrial to nuclear DNA were performed as previously described. Primer sequences used for analysis of gene expression and DNA quantification are as follows: *ACTB* fwd, 5′-CCCAGCACAATGAAGATCAA-3′; *ACTB* rev, 5′-ACATCTGCTGGAAGGTGGAC-3′; *NDUFS4* fwd, 5′-GGAGCTATGACATTGAAGAGAGG-3′; *NDUFS4* rev, 5′-TGCACAGCTGACTTTATTCACA-3′; *NDUFS5* fwd, 5′-GCAGCGGGATAAGCTGATAA-3′; *NDUFS5* rev, 5′-CTTTGACAAGGAGGTTTGTCG-3′; *NDUFB5* fwd, 5′-CTCCGAAAGCAACTCCTGAC-3′; *NDUFB5* rev, 5′-ACTGGAAGCCAAACTCCTCA-3′; *UQCRH* fwd, 5′-CCACAAACTCTTTAACAACTTGAAA-3′; *UQCRH* rev, 5′-CAAATGGTACATCCAAAACCA-3′; *UQCRB* fwd, 5′-GAAAGAGAAGAATGGGCAAAGA-3′; *UQCRB* rev, 5′-GAATTCAAAAACTCCAGCCATT-3′; *UQCRB* -351 bp ChIP fwd, 5′-CTTCCTGCCTGGCACAAAGAGCTGAA-3′; *UQCRB* -351 bp ChIP rev, 5′-GGGAAGAACACAGGTCAGGAATTAGGAGACCA-3′; *UQCRB* -1,728 bp ChIP fwd, 5′-CCAGTAACTATCAGTCATGCTAGCTCCCCCTAATTG-3′; *UQCRB* -1,728 bp ChIP rev, 5′-TCCACCCACGTCAGCCTCCCAAAA-5′; mitochondrial transfer RNA-Leu (URR) fwd, 5′-CACCCAAGAACAGGGTTTGT-3′; mitochondrial transfer RNA-Leu (URR) rev, 5′-TGGCCATGGGTATGTTGTTA-3′; *B2M* fwd, 5′-TGCTGTCTCCATGTTTGATGTATCT-3′; and *B2M* rev, 5′-TCTCTGCTCCCCACCTCTAAGT-3′. All gene expression analyses were normalized against *ACTB*.

ChIP assays

Aliquots of 2.5×10^6 formaldehyde-fixed cells were resuspended in 50 µl nuclei isolation buffer (Abcam). Chromatin was digested by adding 15 U MNase (ThermoFisher) and incubating at 37°C for 5 min. EDTA was added to stop the reaction. Digested chromatin was diluted in immunoprecipitation buffer (20 mM Tris-HCl, pH 8.0, 2 mM EDTA, 150 mM NaCl, 0.1% Triton X-100, and 5 mM sodium butyrate) with EDTA-free protease inhibitors (Millipore) and precleared with Protein G Agarose (Millipore) for 1 h at 4°C. Precleared chromatin was immunoprecipitated overnight at 4°C with antibodies against either ARID5B (NBP1-83622; Novus Biologicals), RNA polymerase II CTD repeat YSPTSPS (phospho-S5; ab5131; Abcam), or histone H3 (dimethyl K9; ab1220; Abcam). Samples were washed and eluted, and cross-links were reversed with a 4-h incubation at 65°C. DNA was precipitated and analyzed by qRT-PCR.

NK cell effector function assays

For determination of NK cell degranulation, ARID5B shRNA and control NK-92 cells were cultured alone or with K562 target cells at a 1:1 ratio for 4 h. Cells were then fixed and analyzed by FACS for surface CD107a expression and intracellular expression of IFN-γ. For additional determination of IFN-γ production, cells were incubated overnight with 5 ng/ml IL-12 (PeproTech) and 50 ng/ml IL-18 (R&D Systems) before staining.

Statistical analysis

Statistics were calculated with GraphPad Prism (v5.0). Data are expressed as the mean ± SEM. Differences between groups were determined by Student's *t* test. P values < 0.05 were considered statistically significant (*P < 0.05, **P < 0.01).

Online supplemental material

Fig. S1 shows OCR and ECAR Seahorse profiles of purified NK cells from two donors that were analyzed freshly after isolation or after a freeze/thaw cycle. Fig. S2 shows a heat map of genes previously implicated in the regulation of mitochondrial biogenesis that was generated using RNA-seq data from sorted subsets of canonical and adaptive NK cells. Fig. S3 depicts Western blot data of ARID5B variant 2 expression in control NK-92 lines and in NK-92 lines transduced with three different shRNAs targeting ARID5B as well as MitoTracker staining for each ARID5B shRNA line compared with empty vector controls. Fig. S4 shows qRT-PCR data of ARID5B expression in NK cells cultured in various stimulatory conditions relative to cell preculture. Table S1 shows GSEA of RNA-seq data for metabolic pathways that were differentially regulated in adaptive NK cells compared with canonical NK cells.

Acknowledgments

We acknowledge expert assistance from the University Flow Cytometry Resource at the University of Minnesota and the University of Minnesota Genomics Center.

This work was supported by grants from the National Institutes of Health (K99HL123638 to F. Cichocki, CA111412 to B.R. Blazar and J.S. Miller, CA65493 to B.R. Blazar and J.S. Miller, CA197292 to M. Felices and J.S. Miller, HL122216 to J.S. Miller, HL11879, and P01 CA142106 to B.R. Blazar), the European Research Council under the European Union's Seventh Framework Program (FP/2007-2013)/ERC Grant Agreement no. 311335, the Swedish Research Council, Norwegian Research Council, Swedish Foundation for Strategic Research, Wallenberg Foundation, Swedish Cancer Foundation, and the Swedish Childhood Cancer Foundation, as well as the Stockholm County Council and Karolinska Institutet Center for Innovative Medicine (to Y.T. Bryceson).

The authors declare no competing financial interests.

Author contributions: F. Cichocki designed experiments, supervised research, analyzed experiments, and wrote the paper. C.-Y. Wu, B. Zhang, and M. Felices performed and analyzed experiments. B. Tesi analyzed experiments. K. Tuininga, P. Dougherty, E. Taras, and P. Hinderlie performed experiments. B.R. Blazar contributed to study design and wrote the paper. Y.T. Bryceson and J.S. Miller contributed to study design, supervised research, and wrote the paper.

Submitted: 28 November 2017
Revised: 8 April 2018
Accepted: 14 June 2018

References

Baba, A., F. Ohtake, Y. Okuno, K. Yokota, M. Okada, Y. Imai, M. Ni, C.A. Meyer, K. Igarashi, J. Kanno, et al. 2011. PKA-dependent regulation of the histone lysine demethylase complex PHF2-ARID5B. *Nat. Cell Biol.* 13:668–675. https://doi.org/10.1038/ncb2228

Bantug, G.R., M. Fischer, J. Grählert, M.L. Balmer, G. Unterstab, L. Develioglu, R. Steiner, L. Zhang, A.S.H. Costa, P.M. Gubser, et al. 2018. Mitochondria-Endoplasmic Reticulum Contact Sites Function as Immunometabolic Hubs that Orchestrate the Rapid Recall Response of Memory CD8+ T Cells. *Immunity.* 48:542–555.e6. https://doi.org/10.1016/j.immuni.2018.02.012

Buck, M.D., D. O'Sullivan, R.I. Klein Geltink, J.D. Curtis, C.H. Chang, D.E. Sanin, J. Qiu, O. Kretz, D. Braas, G.J. van der Windt, et al. 2016. Mitochondrial Dynamics Controls T Cell Fate through Metabolic Programming. *Cell.* 166:63–76. https://doi.org/10.1016/j.cell.2016.05.035

Champagne, D.P., K.M. Hatle, K.A. Fortner, A. D'Alessandro, T.M. Thornton, R. Yang, D. Torralba, J. Tomás-Cortázar, Y.W. Jun, K.H. Ahn, et al. 2016. Fine-Tuning of CD8(+) T Cell Mitochondrial Metabolism by the Respiratory Chain Repressor MCJ Dictates Protection to Influenza Virus. *Immunity.* 44:1299–1311. https://doi.org/10.1016/j.immuni.2016.02.018

Cichocki, F., S. Cooley, Z. Davis, T.E. DeFor, H. Schlums, B. Zhang, C.G. Brunstein, B.R. Blazar, J. Wagner, D.J. Diamond, et al. 2016. CD56dimCD57+NKG2C+ NK cell expansion is associated with reduced leukemia relapse after reduced intensity HCT. *Leukemia.* 30:456–463. https://doi.org/10.1038/leu.2015.260

Claussnitzer, M., S.N. Dankel, K.H. Kim, G. Quon, W. Meuleman, C. Haugen, V. Glunk, I.S. Sousa, J.L. Beaudry, V. Puviindran, et al. 2015. FTO Obesity Variant Circuitry and Adipocyte Browning in Humans. *N. Engl. J. Med.* 373:895–907. https://doi.org/10.1056/NEJMoa1502214

Corat, M.A., H. Schlums, C. Wu, J. Theorell, D.A. Espinoza, S.E. Sellers, D.M. Townsley, N.S. Young, Y.T. Bryceson, C.E. Dunbar, and T. Winkler. 2017. Acquired somatic mutations in PNH reveal long-term maintenance of adaptive NK cells independent of HSPCs. *Blood.* 129:1940–1946. https://doi.org/10.1182/blood-2016-08-734285

Cunningham, J.T., J.T. Rodgers, D.H. Arlow, F. Vazquez, V.K. Mootha, and P. Puigserver. 2007. mTOR controls mitochondrial oxidative function through a YY1-PGC-1alpha transcriptional complex. *Nature.* 450:736–740. https://doi.org/10.1038/nature06322

Falkenberg, M., M. Gaspari, A. Rantanen, A. Trifunovic, N.G. Larsson, and C.M. Gustafsson. 2002. Mitochondrial transcription factors B1 and B2 activate transcription of human mtDNA. *Nat. Genet.* 31:289–294. https://doi.org/10.1038/ng909

Foley, B., S. Cooley, M.R. Verneris, M. Pitt, J. Curtsinger, X. Luo, S. Lopez-Vergès, L.L. Lanier, D. Weisdorf, and J.S. Miller. 2012. Cytomegalovirus reactivation after allogeneic transplantation promotes a lasting increase in educated NKG2C+ natural killer cells with potent function. *Blood.* 119:2665–2674. https://doi.org/10.1182/blood-2011-10-386995

Gerencser, A.A., A. Neilson, S.W. Choi, U. Edman, N. Yadava, R.J. Oh, D.A. Ferrick, D.G. Nicholls, and M.D. Brand. 2009. Quantitative microplate-based respirometry with correction for oxygen diffusion. *Anal. Chem.* 81:6868–6878. https://doi.org/10.1021/ac900881z

Giménez-Cassina, A., and N.N. Danial. 2015. Regulation of mitochondrial nutrient and energy metabolism by BCL-2 family proteins. *Trends Endocrinol. Metab.* 26:165–175. https://doi.org/10.1016/j.tem.2015.02.004

Gumá, M., A. Angulo, C. Vilches, N. Gómez-Lozano, N. Malats, and M. López-Botet. 2004. Imprint of human cytomegalovirus infection on the NK cell receptor repertoire. *Blood.* 104:3664–3671. https://doi.org/10.1182/blood-2004-05-2058

Haut, S., M. Brivet, G. Touati, P. Rustin, S. Lebon, A. Garcia-Cazorla, J.M. Saudubray, A. Boutron, A. Legrand, and A. Slama. 2003. A deletion in the human QP-C gene causes a complex III deficiency resulting in hypoglycaemia and lactic acidosis. *Hum. Genet.* 113:118–122. https://doi.org/10.1007/s00439-003-0946-0

Huss, J.M., I.P. Torra, B. Staels, V. Giguère, and D.P. Kelly. 2004. Estrogen-related receptor alpha directs peroxisome proliferator-activated receptor alpha signaling in the transcriptional control of energy metabolism in cardiac and skeletal muscle. *Mol. Cell. Biol.* 24:9079–9091. https://doi.org/10.1128/MCB.24.20.9079-9091.2004

Kägi, D., B. Ledermann, K. Bürki, P. Seiler, B. Odermatt, K.J. Olsen, E.R. Podack, R.M. Zinkernagel, and H. Hengartner. 1994. Cytotoxicity mediated by T cells and natural killer cells is greatly impaired in perforin-deficient mice. *Nature.* 369:31–37. https://doi.org/10.1038/369031a0

Kortschak, R.D., P.W. Tucker, and R. Saint. 2000. ARID proteins come in from the desert. *Trends Biochem. Sci.* 25:294–299. https://doi.org/10.1016/S0968-0004(00)01597-8

Lahoud, M.H., S. Ristevski, D.J. Venter, L.S. Jermiin, I. Bertoncello, S. Zavarsek, S. Hasthorpe, J. Drago, D. de Kretser, P.J. Hertzog, and I. Kola. 2001. Gene targeting of Desrt, a novel ARID class DNA-binding protein, causes growth retardation and abnormal development of reproductive organs. *Genome Res.* 11:1327–1334. https://doi.org/10.1101/gr.168801

Larsson, N.G., J. Wang, H. Wilhelmsson, A. Oldfors, P. Rustin, M. Lewandoski, G.S. Barsh, and D.A. Clayton. 1998. Mitochondrial transcription factor A is necessary for mtDNA maintenance and embryogenesis in mice. *Nat. Genet.* 18:231–236. https://doi.org/10.1038/ng0398-231

Lee, J., T. Zhang, I. Hwang, A. Kim, L. Nitschke, M. Kim, J.M. Scott, Y. Kamimura, L.L. Lanier, and S. Kim. 2015. Epigenetic modification and antibody-dependent expansion of memory-like NK cells in human cytomegalovirus-infected individuals. *Immunity.* 42:431–442. https://doi.org/10.1016/j.immuni.2015.02.013

Leong, W.Z., S.H. Tan, P.C.T. Ngoc, S. Amanda, A.W.Y. Yam, W.S. Liau, Z. Gong, L.N. Lawton, D.G. Tenen, and T. Sanda. 2017. ARID5B as a critical downstream target of the TAL1 complex that activates the oncogenic transcriptional program and promotes T-cell leukemogenesis. *Genes Dev.* 31:2343–2360. https://doi.org/10.1101/gad.302646.117

Li, F., Y. Wang, K.I. Zeller, J.J. Potter, D.R. Wonsey, K.A. O'Donnell, J.W. Kim, J.T. Yustein, L.A. Lee, and C.V. Dang. 2005. Myc stimulates nuclearly encoded mitochondrial genes and mitochondrial biogenesis. *Mol. Cell. Biol.* 25:6225–6234. https://doi.org/10.1128/MCB.25.14.6225-6234.2005

Liu, Y., L.M. Reynolds, J. Ding, L. Hou, K. Lohman, T. Young, W. Cui, Z. Huang, C. Grenier, M. Wan, et al. 2017. Blood monocyte transcriptome and epigenome analyses reveal loci associated with human atherosclerosis. *Nat. Commun.* 8:393. https://doi.org/10.1038/s41467-017-00517-4

Lopez-Vergès, S., J.M. Milush, B.S. Schwartz, M.J. Pando, J. Jarjoura, V.A. York, J.P. Houchins, S. Miller, S.M. Kang, P.J. Norris, et al. 2011. Expansion of a unique CD57^{+}NKG2Chi natural killer cell subset during acute human cytomegalovirus infection. *Proc. Natl. Acad. Sci. USA.* 108:14725–14732. https://doi.org/10.1073/pnas.1110900108

Marçais, A., J. Cherfils-Vicini, C. Viant, S. Degouve, S. Viel, A. Fenis, J. Rabilloud, K. Mayol, A. Tavares, J. Bienvenu, et al. 2014. The metabolic checkpoint kinase mTOR is essential for IL-15 signaling during the development and activation of NK cells. *Nat. Immunol.* 15:749–757. https://doi.org/10.1038/ni.2936

Mookerjee, S.A., A.S. Divakaruni, M. Jastroch, and M.D. Brand. 2010. Mitochondrial uncoupling and lifespan. *Mech. Ageing Dev.* 131:463–472. https://doi.org/10.1016/j.mad.2010.03.010

Nabekura, T., and L.L. Lanier. 2016. Tracking the fate of antigen-specific versus cytokine-activated natural killer cells after cytomegalovirus infection. *J. Exp. Med.* 213:2745–2758. https://doi.org/10.1084/jem.20160726

Nicholls, D.G. 2009. Spare respiratory capacity, oxidative stress and excitotoxicity. *Biochem. Soc. Trans.* 37:1385–1388. https://doi.org/10.1042/BST0371385

Perry, S.W., J.P. Norman, J. Barbieri, E.B. Brown, and H.A. Gelbard. 2011. Mitochondrial membrane potential probes and the proton gradient: a practical usage guide. *Biotechniques.* 50:98–115. https://doi.org/10.2144/000113610

Puigserver, P., Z. Wu, C.W. Park, R. Graves, M. Wright, and B.M. Spiegelman. 1998. A cold-inducible coactivator of nuclear receptors linked to adaptive thermogenesis. *Cell.* 92:829–839. https://doi.org/10.1016/S0092-8674(00)81410-5

Redondo-Pachón, D., M. Crespo, J. Yélamos, A. Muntasell, M.J. Pérez-Sáez, S. Pérez-Fernández, J. Vila, C. Vilches, J. Pascual, and M. López-Botet. 2017. Adaptive NKG2C+ NK Cell Response and the Risk of Cytomegalovirus Infection in Kidney Transplant Recipients. *J. Immunol.* 198:94–101. https://doi.org/10.4049/jimmunol.1601236

Saeed, S., J. Quintin, H.H. Kerstens, N.A. Rao, A. Aghajanirefah, F. Matarese, S.C. Cheng, J. Ratter, K. Berentsen, M.A. van der Ent, et al. 2014. Epigenetic programming of monocyte-to-macrophage differentiation and trained innate immunity. *Science.* 345:1251086. https://doi.org/10.1126/science.1251086

Schlums, H., F. Cichocki, B. Tesi, J. Theorell, V. Beziat, T.D. Holmes, H. Han, S.C. Chiang, B. Foley, K. Mattsson, et al. 2015. Cytomegalovirus infection drives adaptive epigenetic diversification of NK cells with altered signaling and effector function. *Immunity.* 42:443–456. https://doi.org/10.1016/j.immuni.2015.02.008

Schlums, H., M. Jung, H. Han, J. Theorell, V. Bigley, S.C. Chiang, D.S. Allan, J.K. Davidson-Moncada, R.E. Dickinson, T.D. Holmes, et al. 2017. Adaptive NK cells can persist in patients with *GATA2* mutation depleted of stem and progenitor cells. *Blood.* 129:1927–1939. https://doi.org/10.1182/blood-2016-08-734236

Sentman, C.L., J.R. Shutter, D. Hockenbery, O. Kanagawa, and S.J. Korsmeyer. 1991. bcl-2 inhibits multiple forms of apoptosis but not negative selection in thymocytes. *Cell.* 67:879–888. https://doi.org/10.1016/0092-8674(91)90361-2

Sun, J.C., J.N. Beilke, and L.L. Lanier. 2009. Adaptive immune features of natural killer cells. *Nature.* 457:557–561. https://doi.org/10.1038/nature07665

van der Windt, G.J., B. Everts, C.H. Chang, J.D. Curtis, T.C. Freitas, E. Amiel, E.J. Pearce, and E.L. Pearce. 2012. Mitochondrial respiratory capacity is a critical regulator of CD8+ T cell memory development. *Immunity.* 36:68–78. https://doi.org/10.1016/j.immuni.2011.12.007

van der Windt, G.J., D. O'Sullivan, B. Everts, S.C. Huang, M.D. Buck, J.D. Curtis, C.H. Chang, A.M. Smith, T. Ai, B. Faubert, et al. 2013. CD8 memory T cells have a bioenergetic advantage that underlies their rapid recall ability. *Proc. Natl. Acad. Sci. USA.* 110:14336–14341. https://doi.org/10.1073/pnas.1221740110

Vivier, E., D.H. Raulet, A. Moretta, M.A. Caligiuri, L. Zitvogel, L.L. Lanier, W.M. Yokoyama, and S. Ugolini. 2011. Innate or adaptive immunity? The example of natural killer cells. *Science.* 331:44–49. https://doi.org/10.1126/science.1198687

Whitson, R.H., T. Huang, and K. Itakura. 1999. The novel Mrf-2 DNA-binding domain recognizes a five-base core sequence through major and minor-groove contacts. *Biochem. Biophys. Res. Commun.* 258:326–331. https://doi.org/10.1006/bbrc.1999.0643

Whitson, R.H., W. Tsark, T.H. Huang, and K. Itakura. 2003. Neonatal mortality and leanness in mice lacking the ARID transcription factor Mrf-2. *Biochem. Biophys. Res. Commun.* 312:997–1004. https://doi.org/10.1016/j.bbrc.2003.11.026

Zhang, T., J.M. Scott, I. Hwang, and S. Kim. 2013. Cutting edge: antibody-dependent memory-like NK cells distinguished by FcRγ deficiency. *J. Immunol.* 190:1402–1406. https://doi.org/10.4049/jimmunol.1203034